Check for updates

Enhancing the reliability of dyes for color filters through TiO₂ adsorption: comprehensive identification of factors affecting photocatalysis†

Wan Soo Kim,‡[a] So Jeong Park,‡[a] Tae Gyu Hwang,[b] Hong Mo Kim, [iD][c] Hyun Kyu Lee,[a] Suhyeon Kim,[a] Woo Jin Choi,[a] Jun Ho Yoon,[a] Yoo Sang Kim,[a] Dong Jun Lee,[a] Seong Hyun Jang,[d] Jin Young Kim [iD] *[a] and Jae Pil Kim [iD] *[a]

The reliability of materials used in color filters for CMOS image sensors and TVs is crucial for ensuring high image quality. However, previous studies have revealed shortcomings in the reliability of these materials, especially in terms of thermal and photostability, due to their intrinsic properties. This necessitates the development of novel materials for color filters. Here, we present a novel strategy to improve the reliability of color filters by fabricating a hybrid material in which dye is adsorbed onto TiO₂, which is well known to promote the photodegradation of organic materials. We synthesized three dyes – perylene, DPP, and azo-based – and analyzed the photophysical properties and reliability of both the individual compounds and the resulting hybrid materials. The hybrid material incorporating perylene-based dye demonstrated enhanced photostability, whereas those with DPP and azo-based dyes exhibited contrasting outcomes. Our study investigated the impact of the dyes' photophysical properties and the amount of TiO₂ on the generation of radicals. Additionally, we conducted a quantitative analysis to explore the influence of radical generation on the photostability of the hybrid materials. Lastly, we observed a significant improvement in the thermal stability of the dyes as the amount of TiO₂ increased. Notably, only the perylene-based hybrid material exhibited enhancements in both photostability and thermal stability. Consequently, we determined the optimal dye moiety for a hybrid material and identified the factors influencing photocatalysis, as well as specific factors enhancing the material's reliability.

1. Introduction

The color filter is a device that reproduces colors by transmitting red, green, and blue light, significantly impacting the performance of LCD TVs and image sensors.[1–3] In recent years, its application has expanded to OLED TVs and other fields, necessitating additional research to improve the color filter performance.[4,5] Pigments and dyes are used as materials for color filters, with pigments excelling in reliability but having weak optical properties, and dyes displaying excellent optical

[a] *Department of Materials Science and Engineering, Seoul National University, 151-744, Republic of Korea. E-mail: jaepil@snu.ac.kr*

[b] *Center for Specialty Chemicals, Korea Research Institute of Chemical Technology (KRICT), Ulsan 44412, Republic of Korea*

[c] *Advanced Institute of Convergence Technology, Suwon 864-1, Republic of Korea*

[d] *Material & Component Convergence R&D Department, Korea Institute of Industrial Technology (KITECH), 15588, Republic of Korea*

† Electronic supplementary information (ESI) available: Details of the compounds' synthesis, characterization, morphology, and reliability test data are described here. See DOI: https://doi.org/10.1039/d3ma00897e

‡ Wansoo Kim and So Jeong Park contributed equally as the first author.

properties but weaker reliability.[6,7] Although preliminary studies have been conducted to develop materials that combine the advantages of pigments and dyes, there are limitations in developing such materials due to their intrinsic properties.[6–8] Therefore, developing novel materials with excellent optical properties and reliability is essential.

Pigment-based color filters have optical property issues: transmittance reduction and low color purity, challenging to overcome due to inherent properties.[6,9] In contrast, while efforts have been made to improve the thermal and photostability of the dyes,[7,8,10] the development of compounds that hardly decompose in the color filter process or operating environment has been challenging.

In previous research, dyes' reliability was enhanced by modifying the dye molecule, such as altering the molecular structure or introducing substituents. To advance our understanding, we employed a novel approach by utilizing a hybrid material that adsorbed the dye onto TiO₂ to color filter. Previous studies on materials adsorbing dye onto TiO₂ have mainly focused on accelerating the photodegradation of dyes through photocatalysis.[11–13] In contrast, several studies have
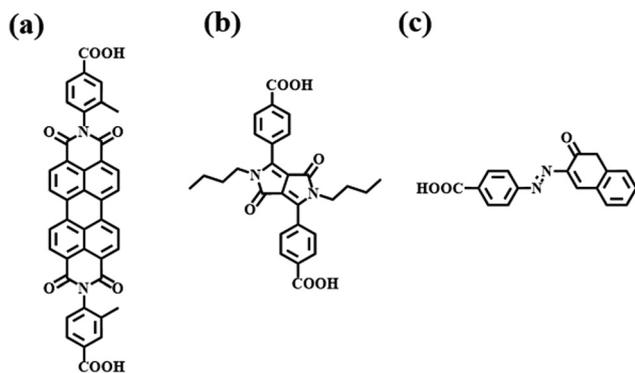
Fig. 1 (a) Structure of **PBI 2**, (b) **DPP-COOH**, (c) **Azo 1**.

reported the potential of TiO_2 to protect dyes from light and heat.[14–17] However, prior studies did not thoroughly investigate the mechanisms by which TiO_2 improves dye photostability and the factors influencing photocatalysis. In this study, we synthesized three dyes (Fig. 1) with transmission in the red region (600–700 nm), adsorbed them onto TiO_2, and meticulously examined the photophysical properties and reliability of the resulting materials. Our investigation comprehensively elucidated the factors influencing photocatalysis, revealed how TiO_2 affects dyes' photo- and thermal stability, and suggested the optimal chromophore for the hybrid material. Notably, our study demonstrated improved thermal and photostability for one of the synthesized dyes when adsorbed onto TiO_2, underscoring the practical utility of this research and proposing a specific and innovative strategy to enhance the reliability of color filters.

2. Experimental section

2.1. Materials

The reagents were purchased from Sigma-Aldrich [poly(methyl methacrylate): average $M_w \sim 15\,000$, poly(styrene-co-methyl methacrylate): average M_w 100 000–150 000, imidazole: purity > 99.5%, zinc acetate: purity > 99.99%, palladium acetate: purity > 98%, cobalt carbonyl: purity > 90%, p-aminobenzoic acid: purity > 99% titanium(IV) chloride: purity > 99.9%, sulfuric acid: purity 95.0–98.0%, methanol: purity > 99.8%], alfa aesar [ammonium hydroxide: purity > 99%], TCI [4-amino-3-methylbenzoicacid: purity > 98%, diisopropyl succinate: purity > 99%, 1-iodobutane: purity > 98%, 4-iodobenzonitrile: purity > 98%, 4-dimethylaminopyridine: purity > 99%, 4,5-Bis(diphenylphosphino)-9,9-dimethylxanthene (Xantphos): purity > 98%, 2-naphthol: purity > 99%], acros organics [3,4,9,10-perylene tetracarboxylic dianhydride: purity > 98%], Samjeon Chemistry [Potassium tert-butoxide: purity > 98%, sodium nitrite: purity > 98%, sodium hydroxide: purity > 98%] and used in the experiments without further purification. All the other solvents were purchased from Samjeon Chemistry.

2.2. Instruments

A Bruker Advance 500 MHz and 850 MHz NMR were used for ^1H NMR to confirm the structure of synthesized compounds,

and N,N-dimethylformamide-d7, toluene-d8, Dichloromethane-d2 was used as a solvent. The molecular weights of the synthesized materials were measured via a matrix-assisted laser desorption ionization mass spectrometer (MALDI-TOF). Fourier-transformed infrared (FT-IR) spectra were collected on a Bruker TENSOR27 spectrometer equipped with an attenuated total reflectance (ATR) cell to confirm the adsorption of TiO_2 and dye (Fig. S16, ESI†).

Spectral characteristics of the compounds were analyzed using SHIMADZU UV1900i, PerkinElmer LS55, Scinco color spectrophotometer-colormate, and JASCO V-770.

Thermal stability of the dyes was analyzed by Thermogravimetric analysis (TGA) by TA instrument's SDT Q600. Lindberg Blue M box furnace was used for heating to explore the thermal stability of the dyes and hybrid materials in the film state. The photostability of the dyes and hybrid materials was analyzed under an incandescent lamp produced by Red100 Lighting Co. Ltd.

Electron spin resonance (ESR) spectroscopies were measured via Bruker's EMXplus-9.5/12/P/L System. The particle size of TiO_2 aggregate in solution was measured via Litesizer™'s Litesizer 500. The X-ray diffraction (XRD, D8 Advance. 2020, Bruker) with Cu Kα radiation (λ = 0.1542 nm) was carried out to measure the crystalline phase of TiO_2 nanoparticles. Morphologies and qualitative compositions were characterized by field-emission scanning electron microscopy (FE-SEM, MERLIN Compact, ZEISS). The surface area was obtained using a Brunauer–Emmett–Teller (BET) analyzer (ASAP 2020 PLUS, Micrometrics).

2.3. Fabrication of hybrid materials in films and solutions

Dyes with various concentrations (0.1, 0.3, 0.5, and 0.7 mM) were dissolved in methyl ethyl ketone (MEK) solutions (5 mL), and TiO_2 was added in various amounts (0, 2, 4, and 8 mg). After stirring for a day, the mixture was filtered through a PTFE syringe filter (0.2 μm of pore size) to remove residual aggregates. PMMA and PS-PMMA polymer binder (20 wt%) were added to the filtered solutions before being drop-cast on quartz plates.[18,19] The cast films were dried for 1 min at 85 °C on the hot plate. The dye concentrations were determined by examining the minimum and maximum concentrations at which the transmittance of the hybrid materials could be used as red materials, considering their solubility, transmittance, and economic feasibility. The TiO_2 concentration was set to have negligible (0, 2 mg in 5 mL solvent) and non-negligible (4, 8 mg in 5 mL solvent) scattering and screening effects.

2.4. Computational calculations

Density functional theory (DFT) and time-dependent density functional theory (TD-DFT) calculations were performed using the Gaussian 16 program based on the 6-31G (d,p)/B3LYP method. The geometrically optimized structures of the synthesized dyes were predicted using this method. To explore the degree of intramolecular charge transfer (ICT), electron density distributions of the highest occupied molecular orbital (HOMO) and lowest unoccupied molecular orbital (LUMO) were calculated. DFT calculations were performed using the Dmol³ module

in the Materials Studios (MS) program (Accelrys Inc., version 2020) to explore the electron density distributions of the HOMO and LUMO of dye-TiO$_2$ complexes. The geometry of bulk TiO$_2$ anatase was obtained from the MS program library, the TiO$_2$ surface was cleaved, and the lattice was controlled. The Perdew and Wang (PWC) functional with double numerical plus polarization (DNP) basis sets were used for the calculations. The S_r value, molecular planarity parameter (MPP), and span of deviation from plane (SDP) were calculated by the Multiwfn program.[20,21]

2.5. Photostability test

Photostability tests of the dyes and hybrid materials in the film state were conducted in a dark box with an incandescent light bulb (10.5 W), in which UV light was filtered. The absorbance of the samples was measured at 1 to 2 h intervals by irradiating them with visible light for 12 h to evaluate the photostability of the samples. For the photostability test, films were fabricated by dissolving the dye at a concentration of 0.1, 0.3, 0.5, and 0.7 mM in 5 mL of solvent and then adding 0, 2, 4, and 8 mg of TiO$_2$, as depicted in Section 2.3.

2.6. Particle size investigation

The synthesized TiO$_2$ was adsorbed on top of carbon tape, and the images were acquired using scanning electron microscopy (SEM). The average particle size was determined by measuring a particle size of more than 100 parts using the ImageJ program.

After dissolving 2, 4, and 8 mg of TiO$_2$ in 5 mL of MEK for a day, the particle size of the aggregates was measured. A quartz cuvette was used, the refractive indices of MEK and TiO$_2$ anatase were input into the instrument, and the particle size was determined by repeating the measurement 60 times.

2.7. Brunauer–Emmett–Teller (BET) surface area analysis

The BET surface areas were determined from the isotherms obtained from the physical adsorption of gas molecules on the nanoparticle surface.[22] The BET equation is given as follows:

$$v = \frac{cv_m x}{(1-x)[1+(c-1)x]}$$

where $x = P/P_0$, and ν is the volume of nitrogen adsorbed per gram of TiO$_2$ nanoparticles at STP, ν_m is the monolayer capacity, and c is related to the heat of adsorption. The equation can be rewritten as follows:

$$\frac{x}{v(1-x)} = \frac{1}{v_m c} + \frac{(c-1)x}{v_m c}$$

BET analysis is performed by plotting $x/v(1-x)$ $vs.$ x, and the values corresponding to c and v_m can be obtained through the slope and y-intercept. The surface area is calculated as follows:

$$A = v_m \sigma_0 N_{av}$$

where σ_0 is the cross-sectional area of the nitrogen liquid density (16.2 Å), and N_{av} is Avogadro's number.

2.8. Electron spin resonance

ESR spectroscopy was used to analyze the generation of radicals produced by irradiating TiO$_2$-dye hybrid materials. All samples were prepared using 5 mL of 0.4 mM of dye solution with TiO$_2$ (0, 2, 4, and 8 mg). Then, samples were irradiated with visible light for 30 min and measured within 5 min. The ESR signal intensities of the hybrid materials were expressed relatively by calculating the difference between the maximum and minimum values of each peak. The peak intensity value of **PBI 2** was set as the reference with a value of 1.

2.9. Thermal stability test

Thermal stability tests were performed on the dye powders from 25 °C to 110 °C and held for 10 min to remove residual solvents. The powders were then heated to 230 °C and held for 1 h to simulate the manufacturing of color filters. Finally, the dyes were heated to 400 °C. The tests were performed under nitrogen conditions at a heating rate of 10 °C min^{-1} using a thermal analyzer system. Absorbance and color difference (ΔE_{ab}) were measured before and after heating to evaluate the thermal stability of the compounds and hybrid materials in the film state. The measurements were taken at 230 °C for 1 h and 300 °C for 5 min in the box furnace.

2.10. Synthesis

Detailed synthetic routes and characterization results of the compounds **PBI 2, DPP-COOH, Azo 1,** and TiO$_2$ (anatase, rutile) and the verification of adsorption between TiO$_2$ and dyes are described in the ESI† (Fig. S1–S15).

2.11. Adsorption investigation

A 0.5 mM (50 mL) solution of three dyes was prepared, and 100 mg of TiO$_2$ was added to the solution. The absorbance was measured after desorbing the dyes from TiO$_2$ using a 0.1 M NaOH aqueous-DMF (1:1) mixed solution. The adsorption amount was determined by dividing the calculated absorbance by the molar extinction coefficient. The physisorption amount was determined by the absorbance using 0.1 M DMF solution. The chemisorption amount was determined by subtracting the physisorption amount from the adsorption amount. All samples were prepared at the same temperature and pH levels. The morphologies of the hybrid materials are described in the ESI.† The adsorption energy between dye and TiO$_2$ was calculated by the MS program.

3. Results and discussion

3.1. Molecular design and analysis

For dyes to be used as a hybrid material in a color filter, it must meet several criteria. Dyes must transmit within a specific wavelength range, demonstrate excellent reliability, and have a structure suitable for adsorption and the introduction of functional groups. After evaluating various candidate groups, three dye moieties, namely perylene, diketopyrrolopyrrole (DPP), and azo, were selected as the most suitable options.

Selecting an appropriate functional group is crucial because its type, number, and position determine the adsorption amount, energy, and photophysical properties.[23–26] Previous studies have explored various functional groups suitable for the adsorption of TiO$_2$ and dyes. Among these, the carboxyl group was chosen due to its ease of introduction, minimal impact on the photophysical properties and structure of the dye, enhanced adsorption amount, higher adsorption energy, and cost-effectiveness.[27,28]

When TiO$_2$ and dye adsorb, both vertical and lying adsorption modes coexist. Dye molecules containing one or two functional groups tend to exhibit vertical adsorption on TiO$_2$, resulting in higher adsorption than lying adsorption.[29] Furthermore, introducing the functional group at the *para* position, rather than the *ortho* or *meta* position, can reduce the steric hindrance and increase the adsorption amount.[30] Based on these considerations, we synthesized three dyes by introducing one or two carboxyl groups at the para position of the benzene ring of the selected dye moieties. The synthesized dyes were **PBI 2**, **DPP-COOH**, and **Azo 1** (Fig. 1).

3.1.1. Computational calculation of the dye molecules. The molecular geometries of the compounds were optimized by using the Gaussian 09 program. The molecular planarity parameter (MPP) and the span of deviation from plane (SDP) were calculated to assess the planarity of the molecules using the Multiwfn program (Fig. 2 and Table 1). Lower MPP and SDP values indicate greater molecular planarity.[20,21] MPP and SDP

Table 1 Molecular planarity parameter (MPP) and span of deviation from plane (SDP) of the compounds

	MPP	SDP
PBI 2	1.186	5.433
DPP-COOH	1.560	5.949
Azo 1	0.766	3.209

decreased in the order of **DPP-COOH** > **PBI 2** > **Azo 1**, indicating that **Azo 1** exhibited the most planar structure, while **DPP-COOH** exhibited the most twisted structure.

Fig. 3 shows the HOMO and LUMO of each dye. S_r values indicating the ratio of the overlapped area between HOMO and LUMO were calculated using the Multiwfn program and shown in Table 2.[31] **PBI 2**, **DPP-COOH**, and **Azo 1** showed S_r values of 0.90, 0.81, and 0.39, respectively, indicating that intramolecular charge transfer (ICT) occurred more in the order of **PBI 2** < **DPP-COOH** < **Azo 1**.

3.1.2. Adsorption investigation. When dyes are physically adsorbed to TiO$_2$, they tend to favor lying structures due to van der Waals forces and hydrogen bonds, whereas chemical bonding results in vertical structure through the dye's functional group.[32] Previous studies have reported the coexistence of lying and vertical adsorption in the TiO$_2$-dye complex due to the competing interactions of physical and chemical adsorption.[33,34] FT-IR analysis indicates the coexistence of physisorption and chemisorption (Fig. S16, ESI†). The ESI† (S1.6) provides detailed assignments of physisorption and chemisorption in FT-IR. SEM images of the fabricated hybrid materials reveal non-uniform particle sizes and rough surfaces, further supporting the coexistence of lying and vertical adsorption (Fig. S17, ESI†).[35] Additionally, a desorption experiment confirmed the physical and chemical adsorption of the dye and TiO$_2$ (Table 3).

In the case of chemisorption, the adsorption energy was calculated using the MS program, and it increased in the order of **DPP-COOH** < **PBI 2** < **Azo 1** (Table 4). Interestingly, **Azo 1**, which has only one functional group, exhibited higher adsorption energy than **PBI 2** and **DPP-COOH**, which have two functional groups. When calculating the adsorption energy of the chemisorption, the optimized structure is the vertical structure in which only one functional group participates in the chemical bond with TiO$_2$ (Fig. 10). The number of functional groups participating in chemisorption is consistent across all hybrid materials. Therefore, it can be analyzed that the increase in adsorption energy is due to the decrease in intermolecular steric hindrance as the planarity of the molecules increases.[36,37] Moreover, since the adsorption amount increased as adsorption energy increased, it is analyzed that the chemisorption amount increased in the order **DPP-COOH** < **PBI 2** < **Azo 1**.[36] Likewise, the physisorption amount followed the same order because the degree to which the dye physically stacks increased as the planarity of the molecule increased.[38] In summary, the adsorption amount increased in the order of **DPP-COOH** < **PBI 2** < **Azo 1**, indicating a correlation between molecule planarity, adsorption energy, and adsorption amount (Tables 1, 3, and 4).
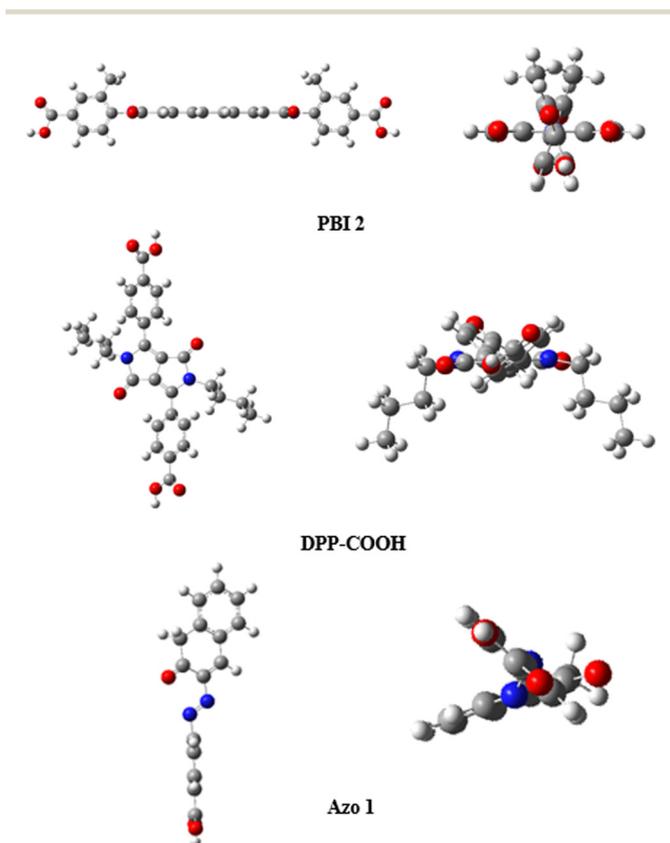

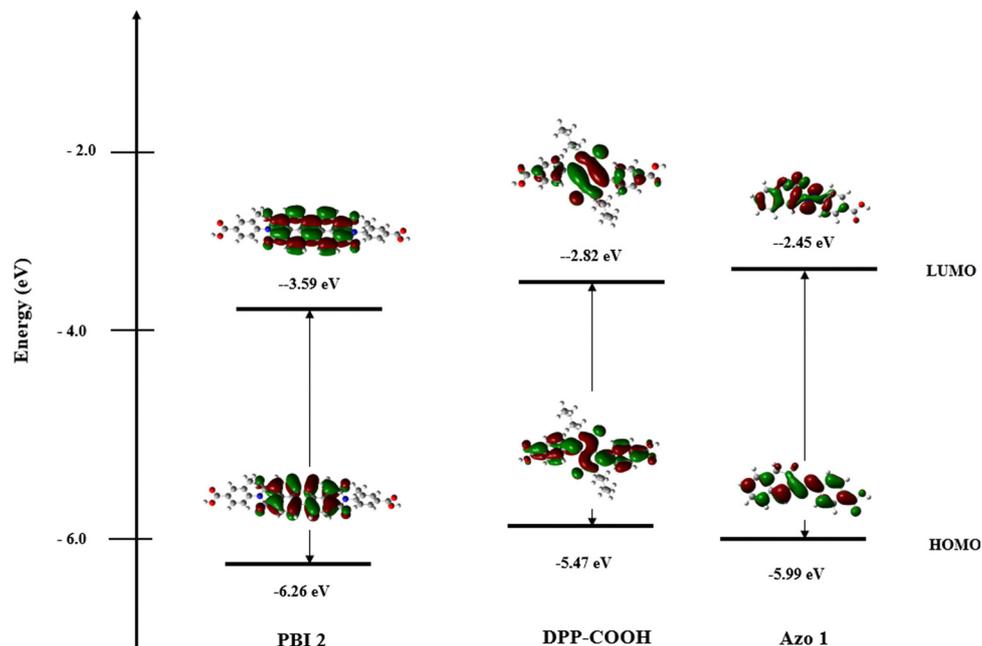**Fig. 2** Geometry-optimized structures of the dyes.

Fig. 3 Frontier molecular orbitals and energy level diagram of the dye molecules.

Table 2 S_r value of the dyes

	PBI 2	DPP-COOH	Azo 1
S_r value	0.90	0.81	0.39

Table 3 Adsorption amount of synthesized dyes on TiO$_2$

	PBI 2	DPP-COOH	Azo 1
Adsorption amount (mM g^{-1})	0.013	0.007	0.020
Chemisorption (approx.)	0.0087	0.0049	0.012
Physisorption (approx.)	0.0043	0.0021	0.0076

*Unit of adsorption amount (mM g^{-1}) indicates adsorbed dye concentration per TiO$_2$ amount.

Table 4 Adsorption energy (E_{ads}) of synthesized dyes on titanium dioxide

	PBI 2	DPP-COOH	Azo 1
Adsorption energy (kcal mol^{-1})	41.1	37.0	78.2

*$E_{ads} = E_{TiO_2} + E_{dye} - E_{TiO_2+dye}$

3.2. Spectral properties

3.2.1. Optical properties of the dyes in the solution. The absorption and transmittance spectra of the dyes in MEK solution at a 1×10^{-5} M concentration are shown in Fig. 4 and Table 5. The maximum absorption wavelengths of **PBI 2**, **DPP-COOH**, and **Azo 1** were 521, 485, and 480 nm, respectively, with corresponding molar extinction coefficients of 36 000, 10 000, and 24 000. All synthesized compounds exhibited a transmittance of over 95% in 600 nm or more, with the highest transmission observed in the red region among visible light.

3.2.2. Optical properties of the hybrid materials in the film. Films were fabricated with varying amounts of TiO$_2$, dye concentration, and film thickness, and their transmittance was measured (Fig. 5). The films showed optimized transmittance at a concentration of 0.7 mM, TiO$_2$ 2 mg in MEK 5 mL, and thickness 0.05 mm. All fabricated films showed a transmittance of over 90% at 600 nm (Table 6). In the case of **DPP-COOH**, due to its low molar extinction coefficient, it showed a transmittance of 48.6% at λ_{max}, rendering it unsuitable for color filters. In contrast, **PBI 2** and **Azo 1** exhibited transmittance of 19.7% and 22.3% at λ_{max}, respectively, indicating their potential as red materials for color filters with appropriate modifications.

3.3. Photostability test

3.3.1. Investigation of factors affecting photocatalysis. In previous studies, much research has focused on promoting the photocatalysis of TiO$_2$.[11–13] However, the photocatalysis process is influenced by various factors, and under specific conditions, the photodegradation of dyes can be inhibited.[14–17] Firstly, when the TiO$_2$ amount exceeds a certain threshold, TiO$_2$ particles aggregate, resulting in light scattering and screening effects. This phenomenon decreases the transmittance of light and obstructs light irradiation, leading to a deterioration of photocatalysis.[14] Additionally, as the dye concentration increases, its adsorption to the photocatalytic active sites on the surface of TiO$_2$ also increases. Consequently, the adsorption of hydroxide ions (OH$^-$) on the TiO$_2$ surface is reduced, resulting in a decreased generation of hydroxyl radicals (OH$^\bullet$) and diminishing the photocatalytic process.[14,39] Furthermore, a higher dye concentration absorbs more light, reducing the
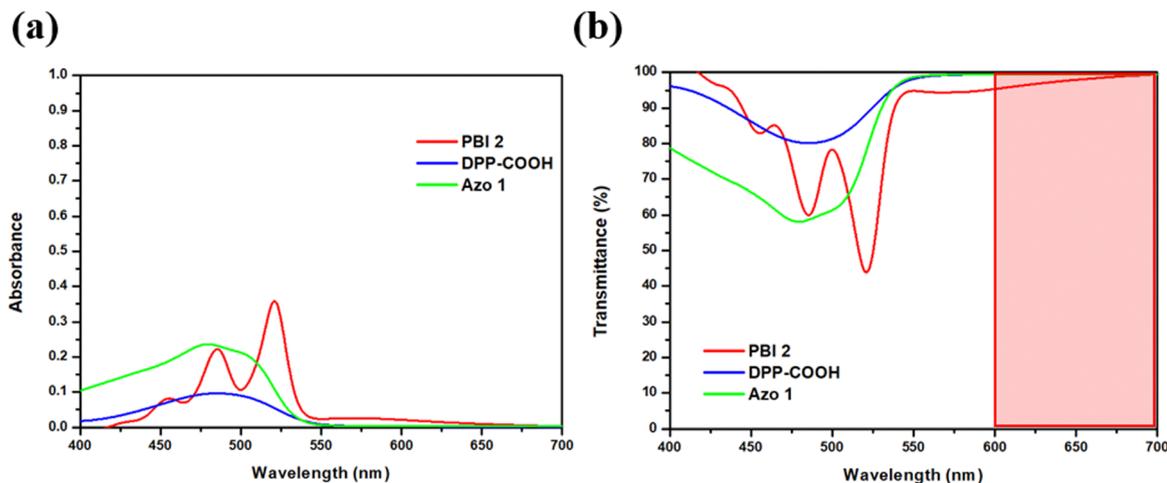
Fig. 4 (a) Absorption and (b) transmittance spectra of the dyes in MEK solution (10^{-5} M).

Table 5 Photophysical properties of the dyes in MEK solution

	$\lambda_{abs,max}$ (nm)	Molar extinction coefficient (L mol^{-1} cm^{-1})	Transmittance at 600 nm (%)
PBI 2	521	36 000	95.3
DPP-COOH	485	9600	99.5
Azo 1	480	24 000	99.5

amount of light reaching the active sites on the TiO$_2$ surface, thus adversely affecting photocatalysis. Another crucial factor influencing photocatalysis is the extent of intramolecular
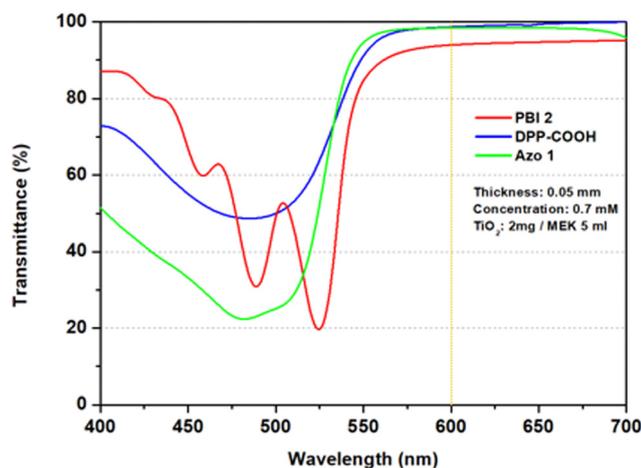

Fig. 5 Absorption and transmittance spectra of the dyes in MEK solution (10^{-5} M).

Table 6 Transmittance of dyes at maximum absorption wavelength and 600 nm

	Transmittance at $\lambda_{abs,max}$ (%)	Transmittance at 600 nm (%)
PBI 2	19.7	93.9
DPP-COOH	48.6	98.7
Azo 1	22.3	98.4

charge transfer (ICT) in the dye molecules. Dyes with a higher degree of charge separation exhibit increased generation of holes and electrons, accelerating the transfer of charges from the dye molecule to TiO$_2$, thereby enhancing photocatalysis. In other words, dyes with less ICT exhibit decreased photocatalytic activity.[40–42]

In summary, the photocatalysis process is influenced by the amount of TiO$_2$, the dye concentration, the extent of dye adsorption, and the degree of ICT. These factors can be expressed through a comprehensive formula below.

$$\text{Photocatalysis} \propto \frac{\text{ICT}}{\text{adsorption amount} \times (\text{dye concentration})} \times f(\text{TiO}_2)$$

(1)

Since the degree of photocatalysis means the degree of radical generation, it can be transformed as follows.

$$\text{Radical generation} \propto \frac{\text{ICT}}{\text{adsorption amount} \times (\text{dye concentration})} \times f(\text{TiO}_2)$$

(2)

In the above equations, (dye concentration) and (TiO$_2$) represent variables. 'f(TiO$_2$)' indicates that the effects on 'photocatalysis' and 'radical generation' vary depending on the concentration of TiO$_2$ (low and high levels) and the specific dye type.

After fabricating hybrid material films by adjusting the concentration of dye and the amount of TiO$_2$ (considering the reasons mentioned in Section 2.3), visible light was irradiated for 12 h, and relative absorbance was measured at intervals of 1 or 2 h (Fig. 6). The photolysis of dyes is shown in Fig. S18 (ESI†).

3.3.2. **Photostability of dyes and hybrid materials in the film.** The average values of the relative absorbance of each dye are depicted as a dotted line (TiO$_2$ = 0 mg), while the average values of the relative absorbance of the hybrid materials (TiO$_2$ = 2, 4, 8 mg) are shown as a solid line in Fig. 6 (Red: **PBI 2**, Green:
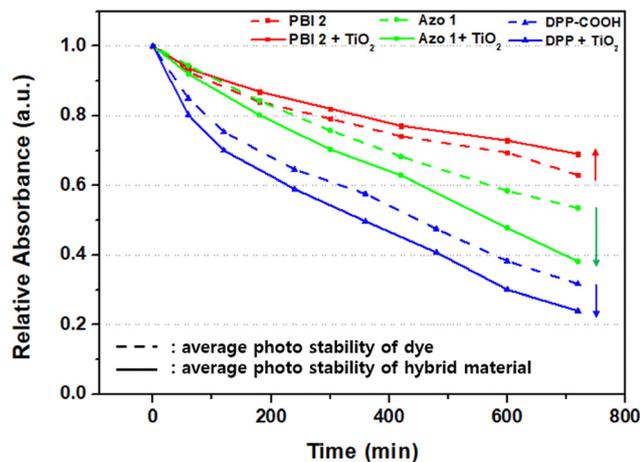
Fig. 6 Average values of relative absorbance of dyes and hybrid materials. *Relative absorbance of dye is averaged across all dye concentrations. *The relative absorbance of hybrid material was averaged across all dye concentrations and TiO_2 amounts.

Azo 1, Blue: **DPP-COOH**). The relative absorbance of the dyes and hybrid materials followed the **DPP-COOH < Azo 1 < PBI 2** order, indicating that perylene-based materials demonstrated the best photostability. Interestingly, for **DPP-COOH** and **Azo 1**, the solid lines were lower than the dotted line, indicating that TiO_2 diminished the photostability of the dye in these hybrid materials. Conversely, in the case of **PBI 2**, the solid line was higher than the dotted line, suggesting that the TiO_2 enhanced the photostability of the dye. To further elucidate the factors contributing to the varying effects of TiO_2 on the photostability of each dye, the relative absorbances after 12 h of light irradiation, depending on the amount of TiO_2, were depicted in Fig. 7.

In the case of **PBI 2**, compared to the photostability of the dye (TiO_2 = 0 mg), the relative absorbance decreased when TiO_2 was 2 mg. However, as TiO_2 increased to 4 and 8 mg, the relative absorbance of the hybrid material increased, indicating improved photostability over that of the dye alone (Fig. 7a). For **DPP-COOH**, when the TiO_2 amount was 2 mg, the relative absorbance decreased compared to that of the dye. However, when the TiO_2 amount was over 2 mg, the relative absorbance increased as TiO_2 increased. Nevertheless, the photostability of the hybrid material was diminished compared to that of the dye at all TiO_2 amounts (Fig. 7b). Interestingly, in the case of **Azo 1**, the relative absorbance decreased as the amount of TiO_2 increased, that is, **Azo 1** was the only material among the three dyes whose photostability only decreased with increasing TiO_2 concentration (Fig. 7c). To elucidate the reason why relative absorbance changed differently depending on the dye type and the amount of TiO_2, we measured the generation of radicals using electron spin resonance (ESR) (Fig. 8, Fig. S19–S21 (ESI†) and Table 7). Additionally, to verify the impact of the amount of TiO_2 on the light scattering and screening effects, we measured the transmittance decrement, the reflectance of the TiO_2 film, and particle size of TiO_2 aggregates at varying TiO_2 amounts (Fig. 9 and Tables 8, 9).
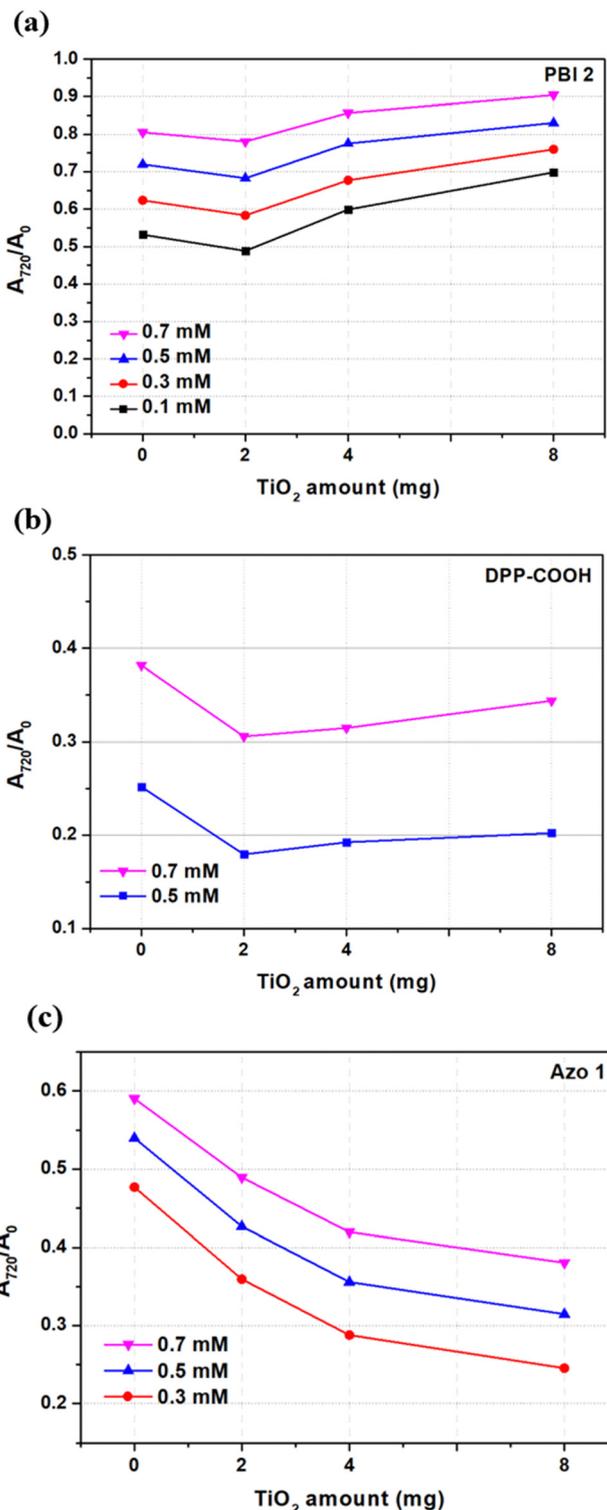

Fig. 7 Relative absorbance by the amount of TiO_2 after 12 h of irradiation of visible light (a) **PBI 2** (b) **DPP-COOH** (c) **Azo 1**. *The absorbance at 0.1 and 0.3 mM concentrations for **DPP-COOH** and 0.1 mM for **Azo 1** were excluded. It is because the molar extinction coefficient of the two dyes was insufficient, making accurate measurements of the absorbance change around the end of irradiation time challenging. Moreover, when TiO_2 was added, the absorbance resembled a noise signal. Therefore, we determined that the photostability test results of the two dyes at that dosage were hard to trust, so excluded.

3.3.3. Electron spin resonance (ESR). The degree of transmittance decrement, reflectance, and particle size increased with the increasing amount of TiO$_2$, indicating a corresponding increase in scattering and screening effects (Tables 8 and 9).[43]

In the case of **PBI 2**, the presence of radicals was detected at 2 mg of TiO$_2$, but as the TiO$_2$ increased to 4 and 8 mg, the ESR signal intensities approached zero, suggesting a significant reduction in radical generation (Fig. 8 and Table 7). At 2 mg of TiO$_2$, a larger portion of irradiated light may have reached the photocatalytic active sites on the TiO$_2$ surface, resulting in radical generation.[14] Conversely, at 4 and 8 mg of TiO$_2$, the diminished radical generation might be due to the increased scattering and screening effects. Additionally, considering that the S_r value for the **PBI 2** molecule is 0.90, indicating limited ICT occurrence, it is plausible that the reduced charge transfer from the dye molecule to TiO$_2$ accounts for the observed minimal ESR signal intensities across all TiO$_2$ amounts (Fig. 8, eqn (2) and Table 2).

In the case of **DPP-COOH**, when the amount of TiO$_2$ was more than 2 mg, radical generation decreased as the amount of TiO$_2$ increased. This could be attributed to the increased scattering and screening effects with increasing TiO$_2$ amounts. Unlike **PBI 2**, the **DPP-COOH**-hybrid material exhibited radical generation at 4 and 8 mg of TiO$_2$. Additionally, ESR signal intensities were higher than those of the **PBI 2**-hybrid material across all TiO$_2$ amounts, indicating a higher radical generation in **DPP-COOH** (Fig. 8). This might be attributed to the smaller adsorption amount of **DPP-COOH** compared to **PBI 2**, and the higher occurrence of ICT in **DPP-COOH** as indicated by its smaller S_r value (eqn (2), Tables 2 and 3).

Among the three hybrid materials, **Azo 1** exhibited the most significant radical generation, and it was the only material in which radical generation increased with increasing TiO$_2$ concentration. This observation indicates that **Azo 1** had the
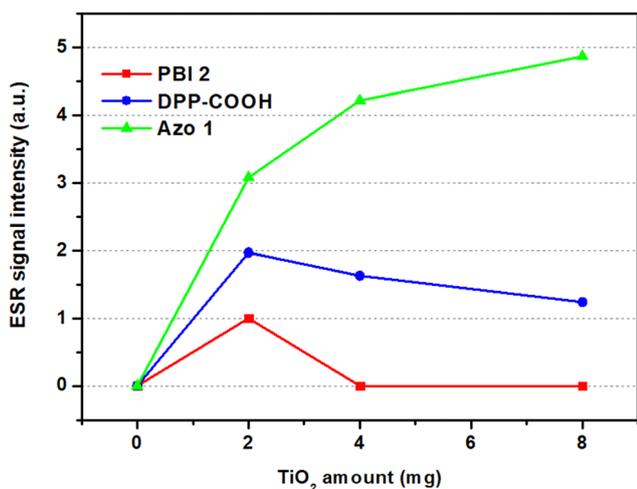

Fig. 8 Electron spin resonance (ESR) signal intensity of the TiO$_2$-dye complexes by the amount of TiO$_2$. *The samples were prepared as depicted in Section 2.8. *The ESR peak intensity of **PBI 2** (TiO$_2$ = 2 mg) was set to 1, and the ESR peak intensities of the remaining hybrid materials were determined.

Table 7 Electron spin resonance (ESR) signal intensity

ESR Signal intensity	0 mg	2 mg	4 mg	8 mg
PBI 2	0	1	0	0
DPP-COOH	0	1.97	1.63	1.24
Azo 1	0	3.09	4.22	4.87

most significant charge transfer to TiO$_2$ among the compounds, given its clear charge separation, indicated by the lowest S_r value (0.39) among the three materials (eqn (2) and Table 2). Furthermore, the increase in radical generation with increasing TiO$_2$ could be attributed to its effective charge transfer in TiO$_2$-dye complexes, even at higher TiO$_2$ amounts. Interestingly, the rate of ESR signal intensity increment decreased as the TiO$_2$ amount increased ($\Delta ESR_{(4\,mg-2\,mg)}$ = 1.13 > $\Delta ESR_{(8\,mg-4\,mg)}$ = 0.65), indicating a decreasing slope in Fig. 8's green line. This decrease might be attributed to the increasing scattering and screening effects accompanying higher TiO$_2$ amounts.

In summary, the role of ICT was evident in the variation of radical generation with TiO$_2$ concentration. For the dyes with limited ICT, radical generation decreased as TiO$_2$ concentration increased, whereas **Azo 1**, characterized by clear ICT, exhibited increased radical generation with greater TiO$_2$ concentration. These results suggest that 'ICT' and 'amount of TiO$_2$' substantially influence radical generation (eqn (2) and Tables 2, 3, 6).

To ascertain the impact of the dye molecule's ICT on charge separation within the TiO$_2$-dye complex and confirm the extent of charge transfer of the hybrid materials from the dye to TiO$_2$, the energy states of the hybrid materials were calculated using the Materials Studio (MS) program.

3.3.4. Computational calculation of the hybrid materials. As shown in Fig. 10, after excitation from HOMO to LUMO, charges remained on the dye in the case of **PBI 2** and **DPP-COOH**-hybrid materials (yellow circles). In contrast, for the **Azo 1**-hybrid material, all charges transferred to TiO$_2$ (red circle), indicating that **Azo 1**, with the most significant ICT, exhibited the most charge transfer to TiO$_2$. Additionally, considering that more radicals were generated in the **DPP-COOH**-hybrid material than in the **PBI 2**-hybrid material, it can be inferred that charge transfer from the dye molecule to TiO$_2$ occurred to a greater extent in the **DPP-COOH**-TiO$_2$ complex than in the **PBI 2**-TiO$_2$ complex (Tables 2 and 7).

In conclusion, we elucidated that the amount of TiO$_2$ and the degree of ICT of dye molecules are the most significant factors affecting the hybrid materials' radical generation.

To explore the effect of the radical generation on the photostability of the hybrid materials, we calculated the average difference in relative absorbance between the hybrid materials (TiO$_2$ = 2, 4, 8 mg) and dyes (TiO$_2$ = 0 mg) for each dye (Fig. 11 and Table 10, relative absorbance data were from Fig. 7).

3.3.5. Photostability change; effect of radical generation. In the case of **PBI 2**, when TiO$_2$ was 2 mg, the photostability of the hybrid material was diminished compared to the photostability of the dye due to the generation of radicals. However, with an increase in the TiO$_2$ to 4 and 8 mg, photostability
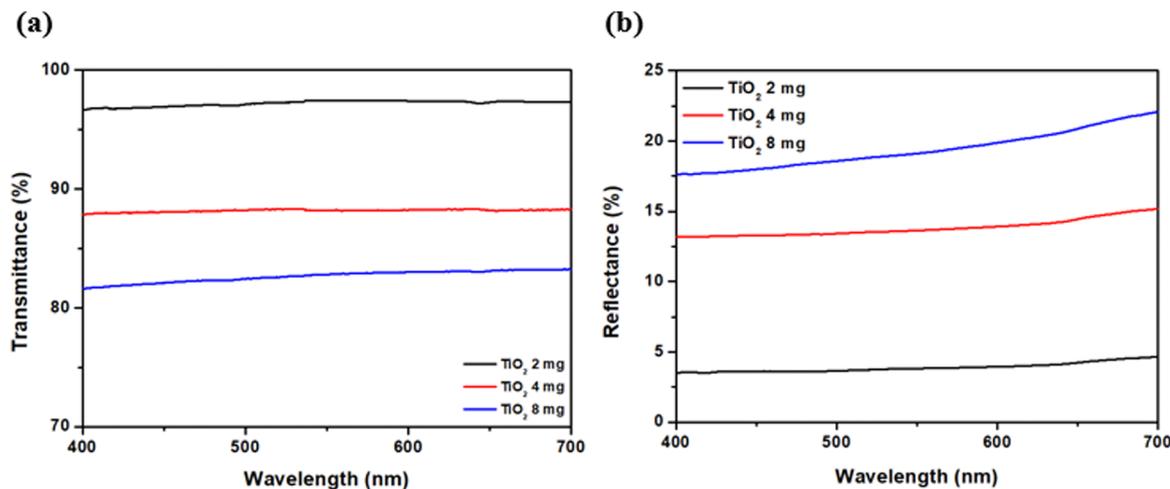
Fig. 9 (a) Transmittance and (b) reflectance of TiO$_2$ film.

Table 8 Average transmittance decrement and reflectance in the visible light region (400–700 nm) of TiO$_2$ film

	2 mg	4 mg	8 mg
Transmittance decrement (%)	−2.78	−11.80	−17.35
Reflectance (%)	3.89	13.81	19.37

Table 9 Particle size of TiO$_2$

	2 mg	4 mg	8 mg
Particle size	120.82 nm	225.98 nm	301.70 nm

*TiO$_2$ was dissolved in 5 ml of MEK (Fig. 9 and Tables 8, 9).

improved due to the screening and scattering effects and the absence of radicals (Section 3.3.3). For **DPP-COOH**, the ESR signal intensity and relative absorbance were 0–1.97–1.63–1.24 and 0–1.86 (−6.75%)–1.74 (−6.32%)–1.20 (−4.37%), respectively, depending on the amount of TiO$_2$. In the case of **Azo 1**, the ESR signal intensity and relative absorbance were 0–3.09–4.22–4.87 and 0–3.24 (−11.76%)–4.99 (−18.13%)–5.84 (−21.22%), respectively, depending on the amount of TiO$_2$ (Tables 7 and 10). Thus, it can be said that ESR signal intensity and relative absorbance differences in all three hybrid materials were quantitatively almost the same. In other words, the graphs in Fig. 8 and 11 exhibited nearly identical formations (x-axis symmetry). This result indicates that the degree of radical generation was the major factor influencing the change in the hybrid materials' relative absorbance (photostability). Moreover, our findings suggest the potential for improving the photostability of dyes by controlling radical generation.

3.4. Thermal stability

3.4.1. Thermal stability of dyes in powder. To ensure the suitability of the materials for color filters, they must exhibit a mass change of less than 5 wt% under the manufacturing process of 230 °C for 1 h.[44] To evaluate the thermal stability of the synthesized dyes, thermogravimetric analysis (TGA) was conducted (Fig. 12 and Table 11). The compounds exhibited mass losses in the order of **PBI 2** (−3.02 wt%) < **Azo 1** (−6.72 wt%) < **DPP-COOH** (−8.36 wt%) at 230 °C for 1 h. **PBI 2** was the only material with a mass loss of <5 wt%, exhibiting excellent thermal stability in powder.

3.4.2. Thermal stability of hybrid materials in film. We fabricated films with varying concentrations of TiO$_2$ (0, 2, 4, 8 mg in 5 ml of MEK) and different dye types using a PS-PMMA binder to evaluate the thermal stability of the hybrid material in the film state. To be used in a color filter, dyes must exhibit a color difference (ΔE_{ab}) less than 3 before and after thermal treatment (230 °C-1 h and 300 °C-5 min) in the film state.[44] The L'a'b' values and ΔE_{ab} results are presented in Tables S1–S3 and Table 12 (ESI†), respectively. In all conditions, ΔE_{ab} of the films followed the order of **DPP-COOH** > **Azo 1** > **PBI 2**, with **PBI 2** demonstrating the best thermal stability among the materials. Interestingly, ΔE_{ab} decreased with increasing amounts of TiO$_2$, indicating that TiO$_2$ enhances the dyes' thermal stability.

Fig. 13 shows the relative absorbance (A/A_0), dividing the absorbance after heat treatment (A) by the initial absorbance (A_0) by the amount of TiO$_2$ and the type of dye. Under all temperature-time conditions and TiO$_2$ amounts, the relative absorbance followed the order of **DPP-COOH** < **Azo 1** < **PBI 2**, with **PBI 2** exhibiting the most excellent thermal stability. Notably, the relative absorbance increased as the amounts of TiO$_2$ increased for all hybrid materials and under all conditions, indicating improved thermal stability. This increase can be attributed to the insulating effect and its ability to restrict oxygen access. TiO$_2$ serves as an insulating barrier that hinders heat transfer between the dye and its surroundings. Additionally, it acts as a barrier to the entry of oxygen and other reactive species into the dye molecules. This protective action helps shield the dye from oxidative degradation, a process induced by oxygen and elevated temperatures. These effects are well-known mechanisms that help maintain the dye at a lower temperature
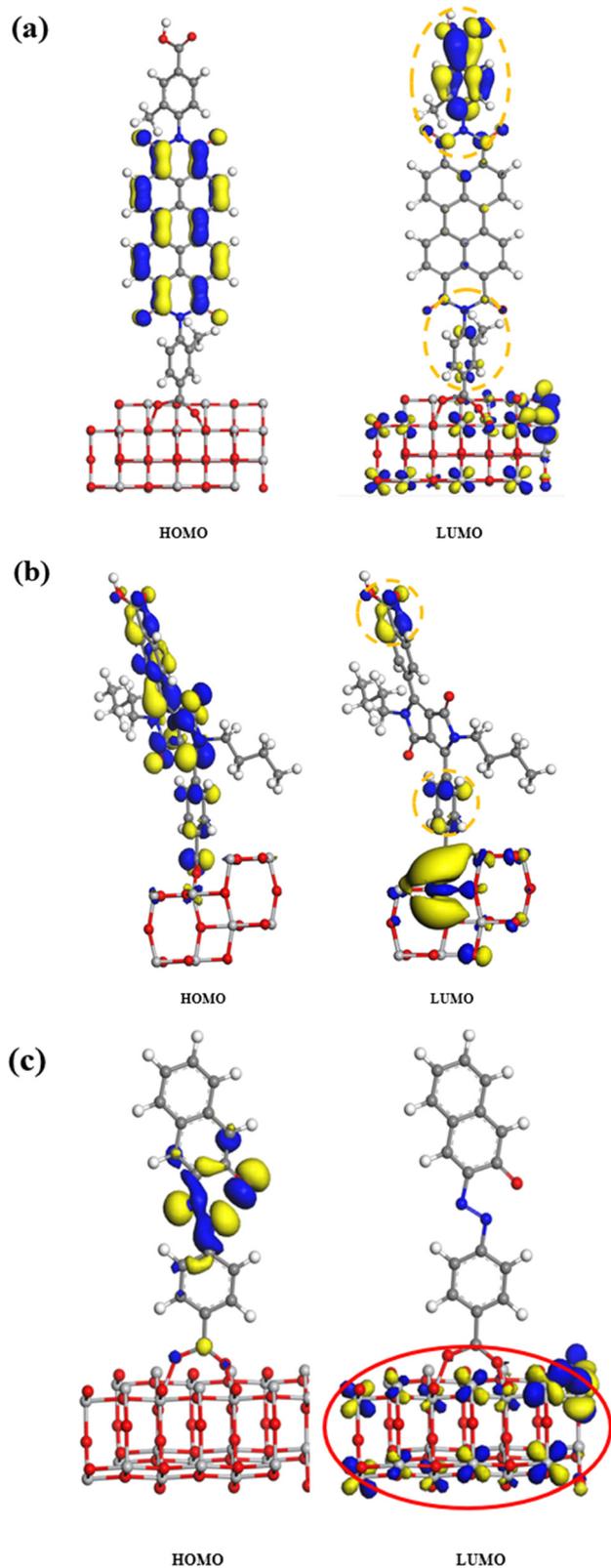
Fig. 10 Energy density distributions of the adsorption system composed of TiO$_2$ and dyes. (a) **PBI 2**, (b) **DPP-COOH** (side view), (c) **Azo 1**.
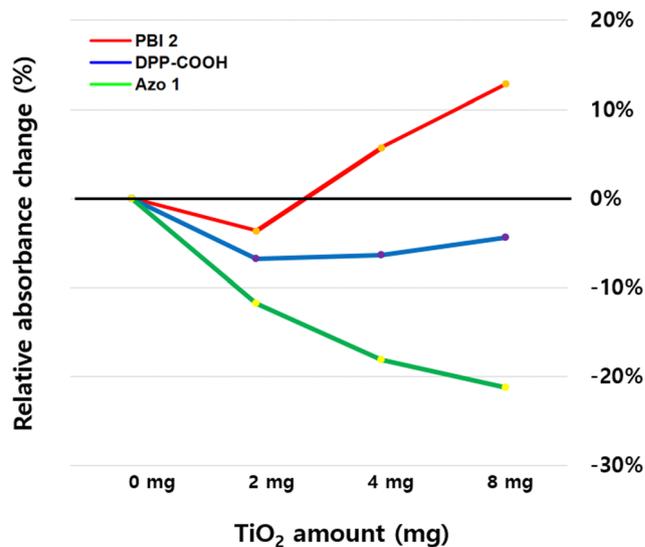

Fig. 11 Difference in relative absorbance of hybrid materials and synthesized dyes.

Table 10 Difference in relative absorbance of hybrid materials and synthesized dyes

	0 mg	2 mg	4 mg	8 mg
PBI 2	0	−3.63% (1)	+5.71%	+12.83%
DPP-COOH	0	−6.75% (1.86)	−6.32% (1.74)	−4.37% (1.20)
Azo 1	0	−11.76% (3.24)	−18.13% (4.99)	−21.22% (5.84)

*The relative absorbance of Fig. 7 was averaged for each amount of TiO$_2$, and then the differences in relative absorbance of dye and hybrid materials were calculated to derive the values in the table.*The decrease of relative absorbance of **PBI 2** when the TiO$_2$ amount is 2 mg (−3.63%) was set to 1.
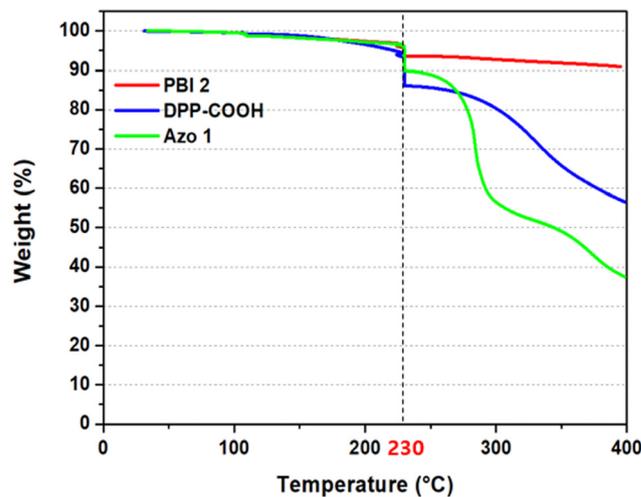

Fig. 12 Thermogravimetric analysis (TGA) of the dyes.

when exposed to heat sources.[45,46] Moreover, as the amount of TiO$_2$ increased, the degree to which the dye was protected from heat increased because the number of TiO$_2$-dye complexes increased as the amount of TiO$_2$ increased.

Table 11 Weight percent decrement of the dyes at 230 °C

	PBI 2	DPP-COOH	Azo 1
Weight decrement at 230 °C (wt%)	−3.02%	−8.36%	−6.72%

Table 12 Color difference (ΔE_{ab}) of the hybrid materials in film after thermal treatment

ΔE_{ab}		0 mg	2 mg	4 mg	8 mg
PBI 2	230 °C-1 h	10.85	8.58	8.44	2.92
	300 °C-5 min	8.71	5.18	2.94	1.29
DPP-COOH	230 °C-1 h	61.63	59.13	50.59	46.09
	300 °C-5 min	54.41	53.35	44.92	41.78
Azo 1	230 °C-1 h	18.50	15.54	11.45	4.96
	300 °C-5 min	12.63	7.95	5.45	1.73

Consequently, the thermal stability of the **PBI 2** dye and the **PBI 2**-hybrid material consistently outperformed the other two materials in all experiments, and the thermal stability of the materials improved with increasing TiO$_2$ concentration. These results further support the enhanced thermal stability of the hybrid material and underscore the potential of **PBI 2** as a candidate for color filter applications, especially when combined with TiO$_2$.

4. Conclusion

In this study, we prepared three hybrid materials by adsorbing perylene, DPP, and azo-based dyes to TiO$_2$ and extensively investigated their adsorption, optical properties, and reliability. The perylene and azo-based hybrid materials exhibited promising potential for application as color filters based on their optical properties. Moreover, the thermal stability of all three hybrid material films significantly improved with increasing amounts of TiO$_2$. Notably, the **Azo 1**-hybrid material generated the most radicals among the materials, while the **PBI 2**-based hybrid material exhibited the least. This difference can be attributed to the ICT of the dye molecules and the charge separation within the TiO$_2$-dye complex. To the best of our knowledge, our study is the first to analyze the factors influencing photocatalysis and radical generation comprehensively and quantitatively. We also identified the optimal conditions for improving thermal and photostabilities, emphasizing the crucial role played by the amount of TiO$_2$ and the charge transfer within the dye and the TiO$_2$-dye complex. Among the three materials, the **PBI 2**-based hybrid material demonstrated the best optical properties and reliability and was the only one that exhibited improved photostability through TiO$_2$. Consequently, these findings provide valuable insights for establishing appropriate conditions to enhance the reliability of color filters and selecting suitable dye moiety in novel hybrid materials.

Author contributions

Wansoo Kim: conceptualization, methodology, investigation, writing - original draft. So Jeong Park: data curation, investigation, funding acquisition. Tae Gyu Hwang: conceptualization, validation. Hong Mo Kim: investigation, data curation. Hyun Kyu Lee: software, validation. Suhyeon Kim: formal analysis, methodology. Woo Jin Choi: figure and table editing. Jun Ho Yoon: software. Yoo Sang Kim: data curation. Dong Jun Lee: visualization. Seong Hyun Jang: software, formal analysis. Jin Young Kim: funding acquisition. investigation, conceptualization. Jae Pil Kim: supervision, project administration, writing review & editing.
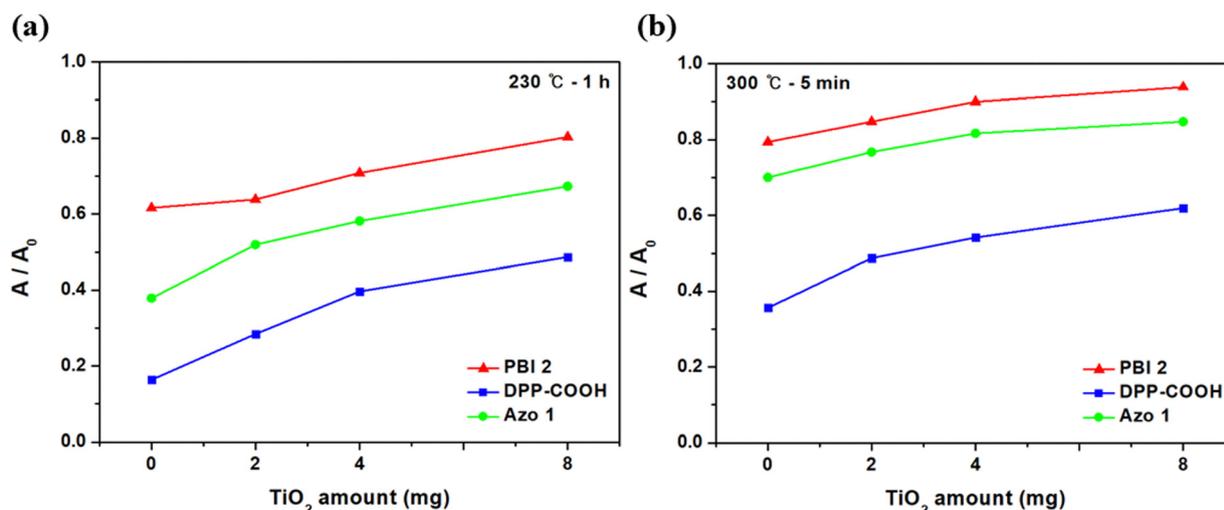
Conflicts of interest

Fig. 13 Relative absorbance by the amount of TiO$_2$ after thermal treatment. (a) 230 °C-1 h, (b) 300 °C-5 min.

Acknowledgements

References

1 A. L. S. O. Edgar González Fernández and L. Javier García Villalba, A multi-channel approach for detecting tampering in colour filter images, *Exp. Syst. Appl.*, 2023, **230**, 15.

2 D. Z. Yanyu Liu, Rencan Nie, Ruichao Hou, Zhaisheng Ding, Weidai Xia and Miao Li, Green fluorescent protein and phase contrast image fusion via Spectral TV filter-based decomposition, *Biomed. Signal Process. Control*, 2023, **79**, 104265.

3 J. W. Namgoong, H. M. Kim, S. H. Kim, S. B. Yuk, J. Choi and J. P. Kim, Synthesis and characterization of metal phthalocyanine bearing carboxylic acid anchoring groups for nanoparticle dispersion and their application to color filters, *Dyes Pigm.*, 2021, **184**, 108737.

4 W. C. Miao, F. H. Hsiao, Y. Sheng, T. Y. Lee, Y. H. Hong, C. W. Tsai, H. L. Chen, Z. Liu, C. L. Lin, R. J. Chung and Z. T. Ye, Microdisplays: Mini-LED, Micro-OLED, and Micro-LED, *Adv. Opt. Mater.*, 2023, 2300112.

5 H. Cho, C. W. Joo, S. Choi, C. M. Kang, B. H. Kwon, J. W. Shin, K. Kim, D. H. Ahn and N. S. Cho, Organic light-emitting diode structure for high color gamut in high-resolution microdisplay: Over 90% color gamut based on BT.2020, *Org. Electron.*, 2022, **101**, 106419.

6 I. Koirala, S. S. Lee and D. Y. Choi, Highly transmissive subtractive color filters based on an all-dielectric metasurface incorporating TiO2 nanopillars, *Optic. Exp.*, 2018, **26**, 14.

7 T. G. H. J. Y. Kim, S. H. Kim, J. W. Namgoong, J. E. Kim, C. Sakong, J. Choi, W. S. Lee and J. P. Kim, Synthesis of high-soluble and non-fluorescent perylene derivatives and their effect on the contrast ratio of LCD color filters, *Dyes Pigm.*, 2017, **136**, 836–845.

8 S. H. K. J. Y. Kim, C. Sakong, S. Choi, H. Jang, K. S. Chang, M. S. Han, J. S. Lee and J. P. Kim, The effect of fluorescence of perylene red dyes on the contrast ratio of LCD color filters, *Dyes Pigm.*, 2016, **131**, 293–300.

9 S. N. D. Wang, W. Jung, H. J. Yang and S. S. Choi, Electrically Wavelength-Controllable Color Filters with High Optical Transmittance Using Heterogeneous Chiral Liquid Crystals, *Adv. Opt. Mater.*, 2023, 2202906.

10 S. H. Kim, J. W. Namgoong, S. B. Yuk, J. Y. Kim, W. Lee, C. Yoon and J. P. Kim, Synthesis and characteristics of metal-phthalocyanines tetrasubstituted at non-peripheral (a) or peripheral (b) positions, and their applications in LCD color filters, *J. Inclusion Phenom. Macrocyclic Chem.*, 2015, **82**, 195–202.

11 G. L. Fen Li, Fuqiang Liu, Jiayu Wu and Sanqiang Yang, Synergetic effect of CQD and oxygen vacancy to TiO2 photocatalyst for boosting visible photocatalytic NO removal, *J. Hazard. Mater.*, 2023, **452**, 15.

12 A. Y. M. Sharma, M. K. Mandal and K. K. Dubey, TiO2 based photocatalysis: a valuable approach for the removal of pharmaceuticals from aquatic environment, *Int. J. Environ. Sci. Technol.*, 2023, **20**, 4569–4584.

13 P. T. Hoai, T. Dai Lam, N. T. Huong and M. T. Van Anh, Removal of ethylene by synthesized Ag/TiO2 photocatalyst under visible light irradiation, *Chemosphere*, 2023, **329**, 138607.

14 M. P. D. Z. Z. Vasiljevic, J. D. Vujancevic, I. Jankovic-Castvan, M. Ognjanovic, N. B. Tadic, S. Stojadinovic, G. O. Brankovic and M. V. Nikolic, Photocatalytic degradation of methylene blue under natural sunlight using iron titanate nanoparticles prepared by a modified sol–gel method, *R. Soc. Open Sci.*, 2020, **7**, 200708.

15 S. O. M. S. Anantha, C. Hu, B. K. Jayanna, N. Reddy, K. Venkatesh, H. B. Muralidhara and R. Naidu, Comparison of the photocatalytic, adsorption and electrochemical methods for the removal of cationic dyes from aqueous solutions, *Environ. Technol. Innovation*, 2020, **17**, 100612.

16 R. S. Devina Rattan Paul, S. P. Nehra and A. Sharma, Effect of calcination temperature, pH and catalyst loading on photodegradation efficiency of urea derived graphitic carbon nitride towards methylene blue dye solution, *RSC Adv.*, 2019, **9**, 15381.

17 Y. X. Zhang, X. D. Hao, F. Li, Z. P. Diao, Z. Y. Guo and J. Li, pH-Dependent Degradation of Methylene Blue via Rational-Designed MnO2 Nanosheet-Decorated Diatomites, *Ind. Eng. Chem. Res.*, 2014, **53**, 6966–6977.

18 T. G. Hwang, G. Y. Kim, J. I. Han, S. Kim and J. P. Kim, Enhancement of Lipid Productivity of Chlorella sp. Using LightConverting Red Fluorescent Films Based on Aggregation-Induced Emission, *ACS Sustainable Chem. Eng.*, 2020, **8**, 15888–15897.

19 Y. Z. Yuhui Dong, J. Song, X. Song and H. Zeng, Recent progress of metal halide perovskite photodetectors, *J. Mater. Chem. C*, 2017, **5**, 11369–11394.

20 T. Lu, Simple, reliable, and universal metrics of molecular planarity, *J. Mol. Model.*, 2021, **27**, 263.

21 F. C. Tian Lu, Multiwfn: A Multifunctional Wavefunction Analyzer, *J. Comput. Chem.*, 2011, **33**, 580–592.

22 P. H. E. Stephen Brunauer and Edward Teller, Adsorption of Gases in Multimolecular Layers, *J. Am. Chem. Soc.*, 1938, **60**, 309–319.

23 J. M. C. Lei Zhang, Anchoring Groups for Dye-Sensitized Solar Cells, *ACS Appl. Mater. Interfaces*, 2015, **7**, 3427–3455.

24 N. Y. Yousuke Ooyama, Joji Ohshita and Yutaka Harima, Impact of the molecular structure and adsorption mode of D–p–A dye sensitizers with a pyridyl group in dye-sensitized solar cells on the adsorption equilibrium constant for dye-adsorption on TiO$_2$ surface, *Phys. Chem. Chem. Phys.*, 2016, **18**, 32992.

25 S. B. Y. W. Lee, J. Choi, H. J. Kim, H. W. Kim, S. H. Kim, B. Kim, M. J. Ko and J. P. Kim, The effects of the number of anchoring groups and N-substitution on the performance of phenoxazine dyes in dye-sensitized solar cells, *Dyes Pigm.*, 2014, 13–21.

26 T. N. K. K. Ladomenou, G. D. Sharma and A. G. Coutsolelos, The importance of various anchoring groups attached on porphyrins as potential dyes for DSSC applications, *RSC Adv.*, 2014, **4**, 21379.

27 H. M. K. J. W. Namgoong, S. H. Kim, S. B. Yuk, J. Choi and J. P. Kim, Synthesis and characterization of metal phthalocyanine bearing carboxylic acid anchoring groups for nanoparticle dispersion and their application to color filters, *Dyes Pigm.*, 2021, **184**, 108737.

28 J. G. Ma, C. R. Zhang, J. J. Gong, B. Yang, H. M. Zhang, W. Wang, Y. Z. Wu, Y. H. Chen and H. S. Chen, The adsorption of α-cyanoacrylic acid on anatase TiO2 (101) and (001) surfaces: A density functional theory study, *J. Chem. Phys.*, 2014, **141**, 234705.

29 W. M. Campbell, A. K. Burrell, D. L. Officer and K. W. Jolley, Porphyrins as light harvesters in the dye-sensitised TiO2 solar cell, *Coord. Chem. Rev.*, 2004, **248**(13–14), 1363–1379.

30 Y. J. Shuaishuai Liu, Yongjie Ding, Xingli Fan, Juan Song, Baoxiu Mi and Zhiqiang Gao, Position engineering of cyanoacrylic-acid anchoring group in a dye for DSSC applications, *Dyes Pigm.*, 2020, 2020.

31 T. Chen, L. Zheng, J. Yuan, Z. An, R. Chen, Y. Tao, H. Li, X. Xie and W. Huang, Understanding the Control of Singlet-Triplet Splitting for Organic Exciton Manipulating: A Combined Theoretical and Experimental Approach, *Sci. Rep.*, 2015, **5**, 10923.

32 C. Anselmi, E. Mosconi, M. Pastore, E. Ronca and F. De Angelis, Adsorption of organic dyes on TiO2 surfaces in dye-sensitized solar cells: interplay of theory and experiment, *Phys. Chem. Chem. Phys.*, 2012, **14**, 15963–15974.

33 R. J. Maurer, V. G. Ruiz, J. Camarillo-Cisneros, W. Liu, N. Ferri, K. Reuter and A. Tkatchenko, Adsorption structures and energetics of molecules on metal surfaces: Bridging experiment and theory, *Prog. Surf. Sci.*, 2016, **91**, 72–100.

34 S. C. A. C. C. Wamser, Adsorption and Photoactivity of Tetra(4-carboxyphenyl)porphyrin (TCPP) on Nanoparticulate TiO2, *J. Phys. Chem. B*, 2000, **104**, 3624–3629.

35 K. J. Hwang, W. G. Shim, Y. Kim, G. Kim, C. Choi, S. O. Kang and D. W. Cho, Dye adsorption mechanisms in TiO2 films, and their effects on the photodynamic and photovoltaic properties in dye-sensitized solar cells, *Phys. Chem. Chem. Phys.*, 2015, **17**, 21974.

36 S. S. Pongthep Prajongtat, Somkiat Nokbin, Koichi Nakajima, Koichiro Mitsuke and Supa Hannongbua, Density functional theory study of adsorption geometries and electronic structures of azo-dye-based molecules on anatase TiO2 surface for dye-sensitized solar cell applications, *J. Mol. Graphics Modell.*, 2017, **76**, 551–561.

37 J. C. S. H. Kim, C. Sakong, J. W. Namgoong, W. Lee, D. H. Kim, B. Kim, M. J. Ko and J. P. Kim, The effect of the number, position, and shape of methoxy groups in triphenylamine donors on the performance of dye-sensitized solar cells, *Dyes Pigm.*, 2015, 390–401.

38 S. Kundu, M. H. Lee, S. H. Lee and S. W. Kang, In Situ Homeotropic Alignment of Nematic Liquid Crystals Based on Photoisomerization of Azo-Dye, Physical Adsorption of Aggregates, and Consequent Topographical Modification, *Adv. Mater.*, 2013, **25**, 3365–3370.

39 I. M. Anila Ajmal, R. Naseem Malik, H. Idriss and M. Amtiaz Nadeem, Principles and mechanisms of photocatalytic dye degradation on TiO2 based photocatalysts: a comparative overview, *RSC Adv.*, 2014, **4**, 37003.

40 T. W. Chenglu Zhu, Yang Wei, Liang Wang, Min Lu, Yupeng Yuan, Lisha Yin and Ling Huang, Unravelling intramolecular charge transfer in donor–acceptor structured g-C3N4 for superior photocatalytic hydrogen evolution, *J. Mater. Chem. A*, 2021, **9**, 1207.

41 M. Y. Yanghee Kim, TiO2/Y-Zeolite encapsulating intramolecular charge transfer molecules: a new photocatalyst for photoreduction of methyl orange in aqueous medium, *J. Mol. Catal. A: Chem.*, 2001, **168**, 257–263.

42 L. Z. Nan Wang, Yingping Huang, Yuanbin She, Yanmin Yu and Heqing Tang, Drastically enhanced visible-light photocatalytic degradation of colorless aromatic pollutants over TiO2 via a charge-transfer-complex path: A correlation between chemical structure and degradation rate of the pollutants, *J. Catal.*, 2009, **266**, 199–206.

43 T. L. H. W. T. Huang and Dyes Amount, and Light Scattering Influence on the Photocurrent Enhancement of Titanium Dioxide Hierarchically Structured Photoanodes for Dye-Sensitized Solar Cells, *Coatings*, 2020, **2020**(10), 13.

44 S. H. K. J. W. Namgoong, S. W. Chung, Y. H. Kim, M. S. Kwak and J. P. Kim, Aryloxy- and chloro-substituted zinc(II) phthalocyanine dyes: Synthesis, characterization, and application for reducing the thickness of color filters, *Dyes Pigm.*, 2018, **154**, 128–136.

45 Y.-m Z. Lu-wei Shen, Pei-gen Zhang, Jin-jie Shi and Zheng-ming Sun, Effect of TiO2 pigment gradation on the properties of thermal insulation coatings, *Int. J. Miner., Metall. Mater.*, 2016, 23.

46 S. K. Jia, Z. O. Yong, J. Y. Xu, W. A. Jing and Y. U. Lei, Effect of TiO2 content on properties of Al2O3 thermal barrier coatings by plasma spraying, *Trans. Nonferrous Met. Soc. China*, 2015, **25**, 175–183.